Catal Lett (2007) 119:159–164
DOI 10.1007/s10562-007-9214-6

One-pot Encapsulation of Pt Nanoparticles into the Mesochannels of SBA-15 and their Catalytic Dehydrogenation of Methylcyclohexane

Aibing Chen · Weiping Zhang · Xiaoyun Li · Dali Tan · Xiuwen Han · Xinhe Bao

Received: 21 May 2007 / Accepted: 11 July 2007 / Published online: 4 August 2007

Abstract Highly dispersed Pt nanoparticles have been confined in the mesochannels of SBA-15 silica by a simple "one-pot" co-assembly method. Metallic Pt can be encapsulated in the mesochannels by changing the amount of Pt ions in the starting materials. The catalytic performances of Pt–SBA-15 were evaluated for methylcyclohexane dehydrogenation. Compared with conventional supported Pt–SiO_2 catalysts, the Pt–SBA-15 catalysts show higher stability. TEM studies show that the confinement effect of ordered mesochannels of SBA-15 may restrict the further growth of Pt nanoparticles during the reaction.

Keywords Pt Nanoparticles · Co-assembly · SBA-15 · Methylcyclohexane · Catalytic dehydrogenation

1 Introduction

Nanostructured materials in confined spaces are the subject of continuing interest because they have unique size-dependent catalytic, nonlinear optical, electrical and other properties, which are significantly different from those in the corresponding bulk substances [1, 2]. Many essential synthesis methods have been developed to prepare various nanopaticles with well-controlled sizes, for example, such materials have been made in colloids [3], porous glasses [4], polymers [5], carbon nanotubes [6] and mesoporous aluminosilicates [7], etc. Among these, to use ordered mesoporous materials as hosts to limit the growth of nanostructured materials in their pores is a relatively promising scheme. The fabrication of metallic Pt nanoparticles with controllable size and shape has become an important topic in nanotechnology for their unique catalytic performance [8]. Normally, Pt nanoparticles or nanowires in porous materials can be synthesized by the following routes: (i) impregnation of the metal salts in the pores of well-made mesoporous materials and subsequent chemical reduction to produce Pt nanocrystals [9]. (ii) ion exchange of the noble metal into SBA-15 functionalized with trimethoxylsilylpropyl-*N*,*N*,*N*-trimethylammonium chloride (TPTAC) and then reduction of this precursor to form Pt nanoparticles within the mesochannels [10]. (iii) Encapsulation of pre-made Pt nanoparticles during the sythesis of the mesoporous materials [11]. However, these methods need at least two or three steps to restrict Pt nanoparticles in the mesoporous matrix. In this paper, we report a novel "one-pot" approach to directly introduce Pt nanopaticles into the mesochannels of SBA-15. No pre-made mesoporous host and Pt nanoparticles are needed in our method, and no extra reduction process of the platinum precursor is needed, either.

Our co-assembly method is based on the $I^+M^-S^+$ scheme for the synthesis of mesoporous host [12]. The positively charged surfactants such as protonated block copolymers [S^+] and cationic inorganic oxide precursors [I^+] are assembled together through the mediator [M^-]. 3-mercaptopropyltrimethoxysilane [MPTMS] with thiol groups are added to modify the cationic precursors [I^+] in order to confine the Pt nanoparticles inside the mesochannels because platinum ions are easy to combined with the thiol groups through strong chemical bonds [13]. The mediator in this case could be the anionic platinum complex and chloride ions. Scheme 1 shows the total synthesis

A. Chen · W. Zhang · X. Li · D. Tan · X. Han · X. Bao (✉)
State Key Laboratory of Catalysis, Dalian Institute of Chemical Physics, Chinese Academy of Sciences, 457 Zhongshan Road, Dalian 116023, China
e-mail: xhbao@dicp.ac.cn

route to obtain monodisperse Pt nanoparticals in SBA-15. The direct co-assembly of MPTMS and tetraethylorthosilicate (TEOS) is preferred over the commonly used post synthesis grafting between surface silanols and functional silylation agents, which provides for a more homogeneous distribution of organic ligands in the framework [14]. After adsorption of platinum ions onto the thiol groups, platinum sulphide analogues can be decomposed into metallic platium and sulfur oxides when heating in air [15]. So, a homogeneous distribution of metallic Pt nanoparticles in the mesochannels of SBA-15 could be expected after calcination at 550 °C to remove the template. These nanocomposites exhibit higher catalytic activity and stability than those of conventional Pt/SiO_2 catalysts in the methylcyclohexane dehydrogenation.

2 Experimental

2.1 Preparation of Pt–SBA-15 Nanocomposites

The molar composition of each final mixture is P123:TEOS:MPTMS:$H_2PtCl_6 \cdot 6H_2O$:HCl:H_2O = 0.017:Q:(1 − Q):(1 − Q)/2:6:180, where Q = 0.98, 0.95 when increasing Pt loadings from 3.1 to 7.5wt%. A typical procedure for preparation of Pt/SBA-15 nanocomposites with Pt loading of 3.1wt% is as follows: 4 g of poly(alkylene oxide) blokcopolymer (Pluronic P-123) were dissolved in 120 ml distilled water and 24 g HCl (37.5%) at 40 °C, then 8.4 g tetraethylorthosilicate (TEOS) were added into the mixture under vigorous stirring. After reaction for 1–3 h, a solution of 3-mercaptopropyltrimethosysilane (MPTMS) (0.16 g), $H_2PtCl_6 \cdot 6H_2O$ (0.21 g) and 3 ml water was added to this mixture. The resultant solution continued to be stirred for *ca.* 20 h at 40 °C, after that the mixture was transferred to the autoclave with Teflon lining and aged at 100 °C for 24 h under static conditions. The solid product was obtained by filtration, washing by water, air-dried at room temperature overnight and calcined at 550 °C to remove the organic groups and to form Pt nanoparticles. The samples are denoted as Pt–SBA-15-3.1 and Pt–SBA-15-7.5, where 3.1 and 7.5 represent the Pt weight precentage, respectively. The samples of 3.0 and 7.5wt% Pt–SiO_2 were obtained by conventional wet impregnation method.

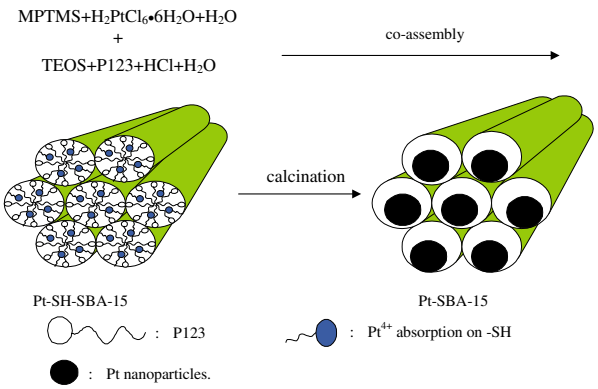

Scheme 1 Preparation process for highly dispersed Pt nanoparticles within the mesochannels of SBA-15

2.2 Characterization

Powder XRD patterns were recorded on Rigaku D/max-2500/PC with Cu Kα radiation in the 2θ range from 0.5–10° or 5–85°. The nitrogen adsorption and desorption isotherms at −196 °C were measured using NOVA 4200e system. The samples were outgassed at 300 °C for 10 h before the measurements. The pore sizes were obtained from the analysis of adsorption branch of the isotherm using the Barrett–Joyner–Halenda (BJH) algorithm. Transmission electron microscopy (TEM) images were collected on a Jeol JEM-2000EX with an acceleration votage of 100 kV. X-ray photoelectron spectroscopy (XPS) was carried out on an Aimcus Specrometer with Mg kα X-ray source. Catalyst dispersion was determined by hydrogen chemisorption at 35 °C on Quantachrome Instruments. Hydrogen isotherms were considered until 35 kPa, as hydrogen chemisorption on the supports was found to be negligible. The values for the platinum dispesion were caculated by assuming a stoichiometry (H:Pt) of 1:1.

2.3 Catalytic Test

The dehydrogenation of methylcyclohexane (MCH) was carried out under atmospheric pressure in a fixed-bed quartz reactor. Prior to reaction, 50 mg catalyst was reduced in situ by hydrogen at 400 °C for 2 h, then the temperature was cooled down to 300 °C, and argon was purged into the system for 30 min before the introduction of MCH. The products were analyzed on-line using a Shimadzu gas chromatography equipped with a 4 m SE-30 column and a TCD. Hydrogen was used as the carrier gas, and toluene was the only product detected.

3 Results and Discussion

3.1 Characterization of Pt/SBA-15 Nanocomposites

Figure 1 shows the N_2 adsorption–desorption isotherms of Pt–SBA-15 nanocomposites. All isotherms are type IV classification with a clear H_1-type hysteresis loop at high

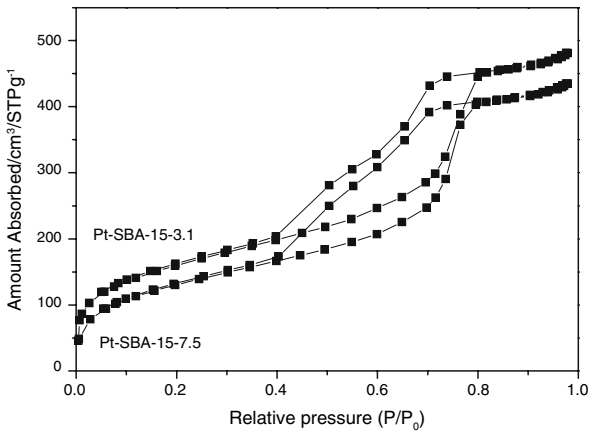

Fig. 1 N_2 Physisorption isotherms of Pt–SBA-15 nanocomposites with different Pt loadings measured at –196 °C

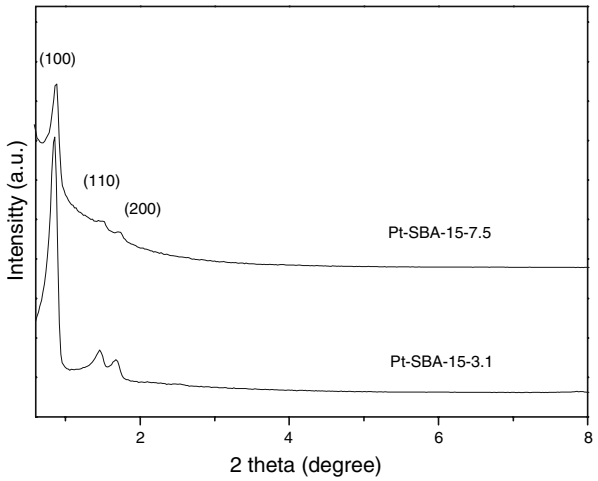

Fig. 2 Low-angle XRD patterns of Pt–SBA-15 nanocomposites with different Pt loadings

relative pressure [16]. A one-step capillary condensation in the adsorption branch indicates uniform mesopores, which are around 8.5 nm for all samples calculated by the BJH model. However, all isotherms exhibit a two-step desorption branch indicating the existence of open and plugged mesopores [17]. The BET surface areas decrease from 702 m^2 per gram of SBA-15 to 665 m^2 per gram of SBA-15 with increasing Pt loadings. These could be attributed to the dispersed Pt nanoparticles in the mesochannels of SBA-15.

The low-angle X-ray diffraction patterns of nanostructured Pt encapsulated in the mesoporous host are displayed in Fig. 2. After calcination, all the XRD patterns display three reflection peaks that can be indexed to the (100), (110) and (200) diffraction lines characteristic of the hexagonal SBA-15 silica [12]. This means the ordered mesostructure is maintained when inclusion of Pt.

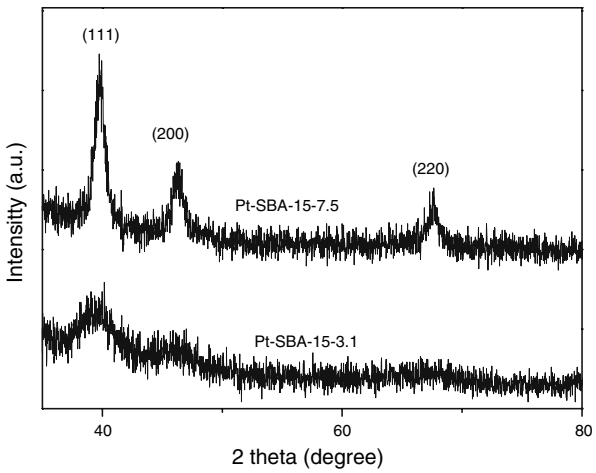

Fig. 3 Wide-angle XRD patterns of Pt–SBA-15 nanocomposites with different Pt loadings

However, the peak intensity in the low-angle region decreases obviously with increasing the Pt contents. This is probably due to the pore filling of nanostructered Pt in the SAB-15 host, which changes the scattering contrast between the pores and the walls of the mesoporous host [7, 10, 18].

The wide-angle XRD patterns of Pt–SBA-15 nanocomposites are shown in Fig. 3. The patterns exhibit three reflection peaks which can be indexed to the (111), (200), and (220) diffraction lines of metallic face-centered cubic Pt [10]. No diffraction peaks of platinum oxides or sulphides are found for each sample. The peaks in Fig. 3 are broad and weak, which may indicate the nanocrystalline nature of Pt in the mesochannels. Along with increasing the Pt contents, the peak intensities of crystalline Pt also increase. The average Pt particle size in SBA-15 host are

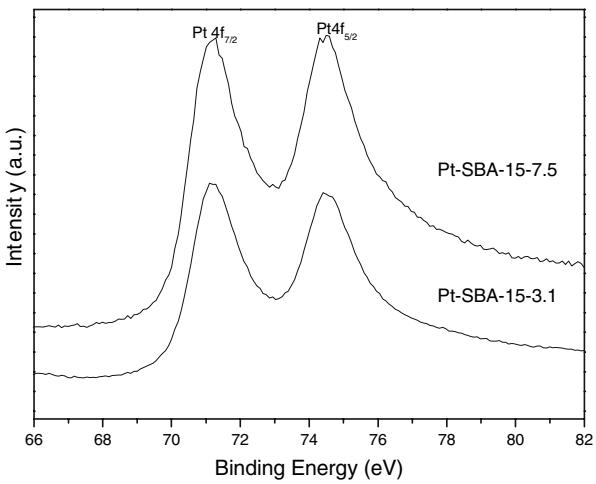

Fig. 4 XPS spectra of Pt–SBA-15 nanocomposites with different Pt loadings focusing on the Pt 4f peaks

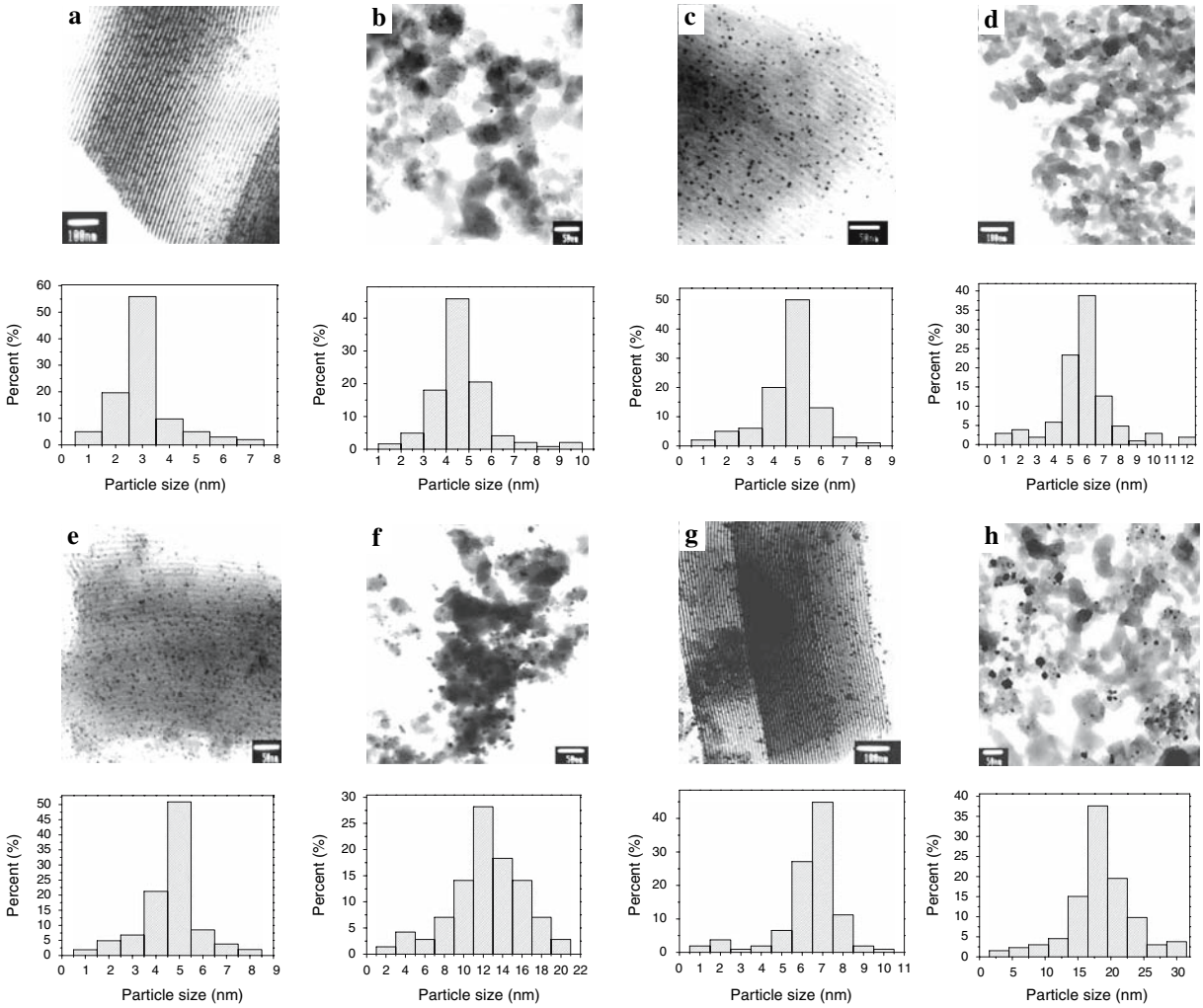

Fig. 5 TEM images and particle size distribution of Pt–SBA-15 (**a**, **c**, **e**, **g**) and Pt–SiO_2 (**b**, **d**, **f**, **h**) with *ca.* 3.0wt%(**a**, **b**, **e**, **f**), and 7.5wt% (**c**,**d**, **g**, **h**) Pt loadings. Images **a**, **b**, **c** and **d** represent the fresh catalysts. Images **e**, **f**, **g** and **h** represent the catalysts after dehydrogenation of methylcyclohexane for 180 min

estimated to be *ca.* 2.4 nm (Pt–SBA-15-3.1) and 4.5 nm (Pt–SBA-15-7.5) from the XRD peak width of Pt (111) reflection by using the Scherrer equation [10, 19].

The presence of metallic Pt nanoparticles in the channels of SBA-15 has also been detected by XPS. Figure 4 indicates that the main peaks with the binding energy of Pt $4f_{5/2}$ at 74.5 eV and Pt $4f_{7/2}$ at 71.2 eV are typical for the non-oxidized Pt^0. The pair of Pt 4f peaks has a spin-orbit splitting of ca. 3.3 eV, which is in good agreement with the predicted value [20]. These further confirm that most Pt nanoparticles confined in SBA-15 host are metallic.

Transmission electron microscopy provides directly observation of the distribution of Pt nanopaticles in the SBA-15. Figure 5 shows the typical TEM images of Pt nanoparticles in SBA-15 with the loadings of 3.1wt% (Fig. 5a) and 7.5wt% (Fig. 5c), respectively. The highly ordered pore structure of SBA-15 is maintained during the formation of Pt

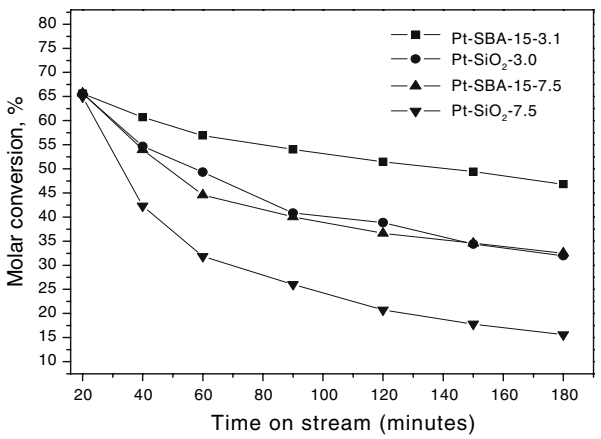

Fig. 6 Time on stream molar percent conversion of methylcyclohexane with Pt–SBA-15 and Pt–SiO_2 catalysts at atmospheric pressure, 300 °C and WHSV of 27.1

Table 1 Pt Particle sizes, H_2 uptakes, dispersions and TOF values for Pt–SBA-15 and Pt–SiO_2 catalysts

Catalyst	Average particle size[a] (±0.5 nm) (fresh catalyst)	Average particle size[a] (±0.5 nm) (final catalyst)	H_2 uptake[b] (μmol g^{-1}) (final catalyst)	Dispersion (final catalyst)	TOF[c] (s^{-1}) (final catalyst)
Pt–SBA-15-3.1	3.1	4.6	14.3	0.36	0.64
Pt–SiO_2-3.0	4.7	12.4	7.8	0.23	0.69
Pt–SBA-15-7.5	4.7	6.4	23.3	0.30	0.21
Pt–SiO_2-7.5	5.8	18.4	10.1	0.15	0.20

[a] Obtain from TEM measurements

[b] Monolayer values extrapolated to $P = 0$ at 308.1 K

[c] Results are given in mole MCH dehydrogenation per mole of platinum surface atoms in the catalyst per second

nanoparticles, and the distribution of Pt particles in the mesoporous host is rather uinform. From the TEM measurement, the average size of Pt is about 3.0 nm and 5.0 nm when the Pt content is 3.1 and 7.5wt%. This is consistent with the XRD results. At the same time, no obvious bulk aggregation of the Pt metal could be found at such Pt loadings.

3.2 Catalytic Evaluation in Methylcyclohexane Dehydrogenation

Methylcyclohexane (MCH) dehydrogenation was chosen as a probe reaction to compare the activity and stability of nanoparticle encapsulation catalysts with the conventional supported catalysts. The catalytic dehydrogenation of methylcyclohexane was carried out using Pt–SBA-15 and Pt–SiO_2 with Pt loading of *ca.* 3.0 and 7.5wt%, respectively. All samples have nearly 100% selectivity of toluene over the entire experimental run. The catalytic activity results are shown in Fig. 6. The initial conversion of MCH is approximately 65.0% for all catalysts, which then decreases with increasing the time on stream. Pt confined in SBA-15 has higher dehydrogenation conversion and stability than that supported on SiO_2 under the same conditions. Figure 5 shows the TEM images of all catalysts before and after methylcyclohexane dehydrogenation. The detailed Pt nanoparticle sizes from TEM measurements are summarized in Table 1. It is found that the average sizes of Pt nanoparticles in all catalysts increase in different degree after methylcyclohexane dehydrogenation, however, the Pt nanoparticle size in SBA-15 increases more slightly than those in SiO_2. The H_2 adsorption uptakes and Pt dispersions were also measured for the samples after 180 min of reaction. It can be seen from Table 1 that the H_2 uptake and Pt dispersion decrease after time on stream of 180 min as the Pt particle size increases accordingly. The dehydrogenation turnover frequencies (TOF) based on the H_2 adsorption and MCH conversion are listed in Table 1. The TOF decreases with increasing Pt loading. The TOF for Pt–SiO_2 and Pt–SBA-15 is similar at the same Pt loading although the average Pt particle size is quite larger in the final Pt–SiO_2 catalyst. This is probably due to the predominance of the contribution of small Pt particles to the catalytic performance in Pt–SiO_2 samples because this reaction is particle size dependent [21]. The smaller particle size and more homogeneous disperison of Pt in SBA-15 may result in its higher catalytic stability in MCH dehydrogenation as the confinement of ordered mesochannels may restrict the further growth of Pt nanoparticles during the reaction.

4 Conclusions

We have developed a new "one-pot" co-assembly method for direct introduction of highly dispersed Pt nanoparticles into the mesochannels of SBA-15. Compared with other methods, for example, functionalized SBA-15, absorption and reduction, this method is simple and also very effective. The distribution of metallic Pt nanoparticles in the SBA-15 host is homogeneous. Most Pt in the synthesis mixture can be confined quantitatively in the mesochannels of SBA-15 by changing the amount of Pt ions in the starting materials. Compared with conventional supported Pt–SiO_2 catalyst, the Pt nanoparticles confined in ordered SBA-15 show higher stability in methylcylohexane dehydrogenation. TEM studies show that the confinement effect of ordered mesochannels of SBA-15 may restrict the further growth of Pt nanoparticles during the reaction.

Acknowledgments We acknowledge the financial support of the National Natural Science Foundation of China (Grant No. 20573106) and the Ministry of Science and Technology of China through the National Key Project of Fundamental Research. We thank the anonymous reviewers for the helpful discussion and suggestions.

References

1. Schmid G (1994) Clusters and collids. VCH, Weihheim

2. Hu J, Odom TW, Lieber CM (1999) Acc Chem Res 32:435
3. Verelst M, Ely TO, Amiens C, Snoeck E, Lecante P, Mosset A (1999) Chem Mater 11:2702
4. Lifshitz E, Yassen M, Bykov L, Dag I, Chaim R (1994) J Phy Chem 98:1459
5. Pileni MP (2000) Pure Appl Chem 72:53
6. Pham-Huu C, Keller N, Estournès C, Ehret G, Ledoux MJ (2002) Chem Commun 1882
7. Gu J, Shi J, You G, Xiong L, Qian S, Hua Z, Chen H (2005) Adv Mater 17:557
8. Narayanan R, El-Sayed MA (2005) J Phys Chem B 109:12663
9. Han Y, Kim JM, Stucky GD (2000) Chem Mater 12:2068
10. Yang C, Liu P, Ho Y, Chiu C, Chao K (2003) Chem Mater 15:275
11. Konya Z, Puntes VF, Kiricsi I, Zhu J, Alivisatos P, Somorjai GA (2002) Catal Lett 81:137
12. Zhao D, Huo Q, Feng J, Chmelka BF, Stucky GD (1998) J Am Chem Soc 120:6024
13. Kang T, Park Y, Yi J (2004) Ind Eng Chem Res 43:1478
14. Walcarius A, Delacote C (2003) Chem Mater 15:4181
15. Mellor JW (1937) A comprehensive treatise on inorganice and theoretical chemistry, vol XVI. Green and CO. Ltd., Longmans
16. Gregg SJ, Sing KSW (1982) Adsorption, surface area and porosity. Academic Press, London
17. Meynen V, Beyers E, Cool P, Vansant EF, Mertens M, Weyten H, Lebedevc OI, Van Tendeloo G (2004) Chem Commun 898
18. Winkler H, Birkner A, Hagen V, Wolf I, Schmechel R, Seggern H, Fischer RA (1999) Adv Mater 11:1444
19. Jenkins R, Snyder RL (1996) Chem Anal 138:90
20. Zhang LX, Shi JL, Yu J, Hua ZL, Zhao XG, Ruan ML (2002) Adv Mater 14:1510
21. Rochefort A, Le Peltier F, Boitiaux JP (1992) J Catal 138:482